Plasma Chemistry and Plasma Processing, Vol. 22, No. 2, June 2002 (© 2002)

Characterization of the Active Species in the Afterglow of a Nitrogen and Helium Atmospheric-Pressure Plasma

S. E. Babayan,[1] G. Ding,[1] G. R. Nowling,[1] X. Yang,[1] and R. F. Hicks[1,2]

Received December 13, 2000; accepted July 31, 2001

The concentrations of the neutral active species in the afterglow of a nitrogen and helium atmospheric-pressure plasma have been determined by optical emission and absorption spectroscopy and by numerical modeling. For operation with 10 Torr N_2 and 750 Torr He, at 15.5 W/cm^3 rf power, 30.4 L/min flow rate, and a neutral temperature of 50°C, the plasma produced 4.8×10^{15} cm^{-3} of ground state nitrogen atoms, $N(^4S)$, 2.1×10^{13} cm^{-3} of $N_2(A\,^3\Sigma_u)$, 1.2×10^{12} cm^{-3} of $N_2(B\,^3\Pi_g)$, and 3.2×10^9 cm^{-3} of $N_2(C\,^3\Pi_u)$. The concentration of nitrogen atoms and metastable state nitrogen molecules, $N_2(A)$, increased gradually with the rf power and the nitrogen partial pressure. Both the model and experiments indicate that ground-state nitrogen atoms are the dominant active species in the afterglow beyond 2.0 ms.

KEY WORDS: Atomic nitrogen; nitrogen plasma; atmospheric pressure plasma.

1. INTRODUCTION

Thin films of nitride materials, such as silicon nitride and gallium nitride, are essential components of many solid-state electronic devices.[1–5] To avoid damaging the nanoscale features in these devices, it is necessary to deposit these films at low temperatures, < 500°C. In this case, radio frequency (rf) or microwave plasmas are used to activate nitrogen or ammonia molecules into species, which can drive the deposition reaction at the desired temperature.[6–9]

The plasma-enhanced chemical vapor deposition (PECVD) of nitride films is normally carried out in reactors operating at pressures below 10 Torr.[6] Researchers investigating the deposition process have suggested that a variety of different species may be involved in the reaction, including

[1]Department of Chemical Engineering, University of California, Los Angeles, California 90095.
[2]To whom all correspondence should be addressed; e-mail: rhicks@ucla.edu

0272-4324/02/0600-0255/0

nitrogen atoms,[10] metastable or excited nitrogen molecules,[11,12] nitrogen ions,[13] and even helium metastables.[14] On the other hand, studies of the neutral afterglow chemistry of low-pressure nitrogen plasmas (primarily microwave discharges) have focused on either measuring the densities of ground-state nitrogen atoms,[15,16] or the densities of the three molecular excited states, $N_2(A\,^3\Sigma_u)$, $N_2(B\,^3\Pi_g)$, and $N_2(C\,^3\Pi_u)$.[17,18] To our knowledge, only one study by Diamy *et al.*[19] characterized all the active species in the afterglow. In that work, at a pressure of ~20 Torr, the concentration of N atoms was found to be several orders of magnitude higher than the metastable nitrogen molecules, with $N_2(A\,^3\Sigma_u)$ being the most abundant of these. However, there is still uncertainty regarding the production of active nitrogen species in the afterglow region of gas discharges employed in nitride PECVD.

We are interested in atmospheric pressure plasmas for thin film deposition, because they may offer certain advantages over low-pressure systems, such as the potential for new reaction chemistry, and the ability to process substrates of almost any size or shape since a vacuum chamber is not required.[20–23] Most studies of atmospheric pressure nitrogen plasmas have been performed with "torches", where the temperature exceeds 500°C.[24–27] Few have investigated the chemistry in the non-equilibrium, low-temperature regime.[28–29] We have developed a noble gas-stabilized, atmospheric pressure plasma source that operates at temperatures below 120°C.[20–22] Approximately 1.5% of nitrogen or oxygen can be added to the noble gas feed to create the desired chemistry. The noble gas can be either helium (ν_{rf} = 13.56 MHz) or argon (ν_{rf} = 27.12 MHz). This homogeneous, capacitive discharge produces a high flux of reactive species.[21,30] High-quality silicon nitride films have been deposited with this source at 1.0 atmosphere and a substrate temperature of 400°C.[31]

In this manuscript, we report on an investigation of the active neutral species in the afterglow of a helium-stabilized, atmospheric-pressure plasma source that is fed with 10 Torr of nitrogen. The concentrations of $N(^4S)$, $N_2(A\,^3\Sigma_u)$, $N_2(B\,^3\Pi_g)$, and $N_2(C\,^3\Pi_u)$ have been measured as functions of time (and distance) in the afterglow by transient optical spectroscopy and numerical modeling. The nitrogen atom concentrations have been recorded using a new technique that we have described in a separate paper.[32] These results indicate that ground-state atomic nitrogen is by far the dominant active intermediate in the downstream region of the discharge, and most likely would dominate the reaction chemistry of the nitride PECVD process.

2. EXPERIMENTAL METHODS

2.1. Apparatus

The gas discharge system employed in these experiments has been described previously in more detail.[32] It consisted of two parallel plate

electrodes separated by a uniform gap of 1.6 mm. The upper half of the plasma source consisted of a powered aluminum electrode measuring 10.2 cm in width and 7.9 cm in length. To maintain the uniform gap downstream of the plasma, a Teflon block, 10.2 cm wide and 1.3 cm long, was mounted just downstream of the upper electrode followed by an aluminum block, 10.2 cm wide and 10.2 cm long. The lower half of the plasma source consisted of a water-cooled stainless steel electrode, 10.2 cm wide and 20.4 cm long, which was grounded. The sides of the device were sealed with quartz windows so that spectroscopic measurements of the plasma and afterglow could be made. The volume of the plasma generated in this configuration was 12.9 cm^3 (10.2 cm wide by 7.9 cm long by 1.6 mm high). The neutral gas temperature in the plasma and afterglow was measured by calculating the rotational temperature of the (3, 0) band of the N_2 first positive emission spectrum from a Boltzmann plot.[33] In the afterglow, the neutral temperature was also checked with an ungrounded thermocouple, 0.8 mm in diameter. The two methods agreed to within 20 K.

The standard conditions for operation of the plasma were 200 W or 15.5 W/cm^3 of 13.56 MHz rf power, a total flow rate of 30.4 L/min, 750 Torr of helium, and 10 Torr of nitrogen. These flow rates produced a linear velocity of 3.7 m/s, corresponding to a Reynolds number of 50, which was within the laminar-flow regime. The helium and nitrogen were both of ultra-high purity (99.999%), while the nitric oxide used for titration was of commercial purity (99%). To further reduce oxygen and water impurities, the helium and nitrogen were passed through an oxygen absorbing purifier (Matheson Gas Products, 6413).

As shown in Fig. 1, the spectroscopic measurements were performed using two configurations of the apparatus. In the first configuration, the discharge was operated in a continuous mode, while sampling the light perpendicular to the flow direction. The light was collected through a 1.2 mm wide slit and onto the entrance slit of the monochromator (Instruments S.A., Triax 320). The monochromator was equipped with a 1200 groove/mm grating, a liquid nitrogen cooled CCD (Instruments S.A., CCD-3000) and a thermoelectrically cooled photo-multiplier tube (PMT) (Hamamatsu, R928P). With the CCD, the monochromator entrance slit was set to 0.05 mm, resulting in a spectral resolution of 0.16 nm. The plasma source was mounted on a linear slide so that profiles of light emission or absorption could be collected by translating it in front of the detection system, resulting in a spatial resolution of 2 mm.

In the second configuration, the discharge was operated in a pulsed mode, and the light emission was sampled parallel to the gas flow direction. Sampling perpendicular to the gas flow direction was avoided since the transit time of the gas was on the order of the sampling time in these experiments. Here, the rf generator (RF Power Products, RF10S) delivered power

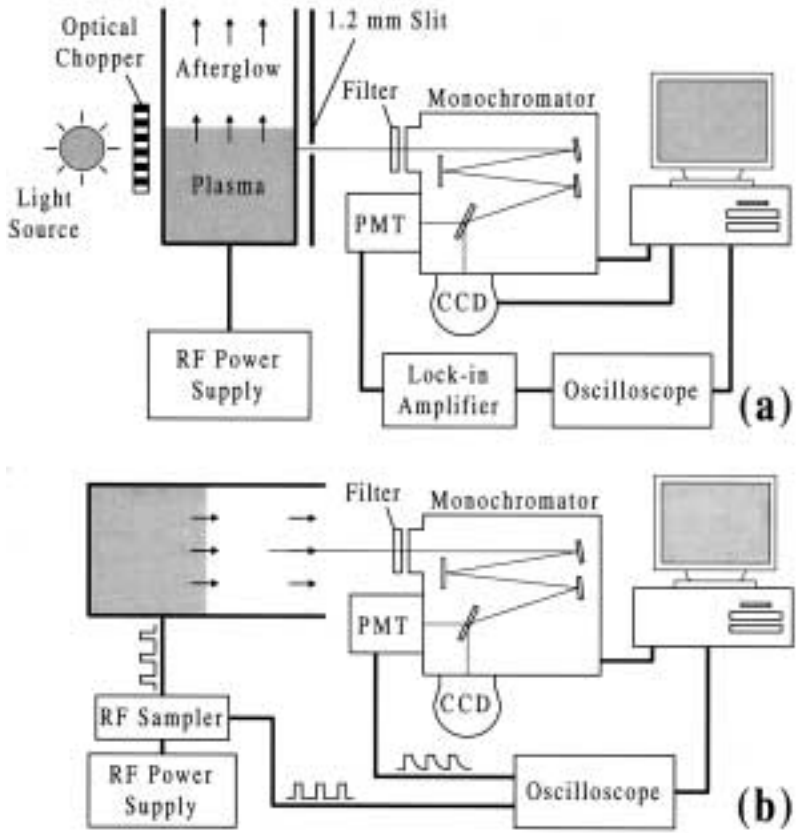

Fig. 1. Schematic of the experimental apparatus used to probe the plasma during (a) continuous and (b) pulsed operation.

in 50 ms pulses with a 20% duty cycle. The decay of the emission from the active species was monitored as a function of time with the PMT, resulting in a resolution of 2.6 μs. The decay time was mapped onto position in the afterglow by using a standard and equivalent method of multiplying the time by the linear velocity of the gas, 3.7 m/s. A time resolution of 2.6 μs corresponded to a spatial resolution of 10 μm. This is a 200-fold improvement over the measurements made during continuous operation.

2.2. $N_2(B\,^3\Pi_g)$

The concentration of $N_2(B)$ inside the plasma was obtained with the configuration shown in Fig. 1a. The $N_2(B)$ concentration was calculated

from its emission intensity as discussed in a previous report.[32] The optical emission was calibrated with a tungsten standard lamp (Oriel, 63976) and the Einstein coefficients were taken from the work of Gilmore *et al.*[34] The total $N_2(B)$ concentration was estimated from the sum of the populations of each vibrational state from $v' = 0$ to 12.

The temporal decay profile of $N_2(B)$ in the afterglow was recorded with the experimental configuration shown in Fig. 1b. A power sampler (Bird, 4273-025) was used to monitor the pulsed voltage signal to the plasma and trigger the oscilloscope (Tektronix, TDS 224). The output of the PMT was fed directly to the oscilloscope, which computed a moving average of 128 decay profiles. To obtain the absolute $N_2(B)$ concentration, the sum of the PMT signals for $v' = 1$ to 12 states at zero time was normalized to the CCD measurements taken at the edge of the discharge during continuous operation at the same conditions. The decay profile for $v' = 0$ was not collected since it was outside the detection range of the PMT. The accuracy of the $N_2(B)$ concentrations reported in this study was estimated to be $\pm 20\%$.

2.3. $N_2(C\,^3\Pi_u)$

The concentration profile of the $N_2(C)$ species was determined in the same fashion as the $N_2(B)$ species described above, using Einstein coefficients from Gilmore *et al.*[34] The population of the $N_2(C)$ vibrational states 0 through 4 were summed to obtain the total concentration. The accuracy of the $N_2(C)$ concentrations was estimated to be $\pm 20\%$.

2.4. $N_2(A\,^3\Sigma_u)$

The $N_2(A)$ concentration was measured in the plasma and the afterglow by absorption at 886 nm with the experimental configuration shown in Fig. 1a. The light source was a second helium and nitrogen atmospheric-pressure plasma with a neutral temperature near 500 K. With this source, the $N_2(A)$ concentration could be determined from an absorption coefficient obtained at the same discharge temperature.[35] The light from the second source was passed through an optical chopper. The absorption at 886 nm was monitored with the PMT detector through a 650 nm high-pass filter. The signals from the PMT and the chopper were fed directly to a lock-in amplifier (Stanford Research, SR830), and the output from the amplifier was monitored with the oscilloscope. These measurements were made with and without nitrogen in the feed to the main plasma source, in order to obtain I and I_0 for calculating the concentration from the Beer–Lambert Law.

During pulsed plasma operation, the $N_2(A)$ concentration was calculated from the $N_2(C)$ concentration (see Section 2.4, above). In the afterglow, a detectable amount of $N_2(C)$ was produced by energy pooling between two $N_2(A)$ molecules, $N_2(A) + N_2(A) \rightarrow N_2(C) + N_2(X)$. The $N_2(C)$ was consumed by radiation and by collisional quenching with helium and nitrogen (Table I). The change in the $N_2(C)$ concentration is given by,

$$\frac{d[N_2(C)]}{dt} = k_{\text{pool}}[N_2(A)]^2 - [N_2(C)](k_{\text{rad}} + k_{q,\text{He}}[\text{He}] + k_{q,N_2}[N_2]) \qquad (1)$$

where $k_{\text{pool}} = 3.0 \times 10^{-10}\ \text{cm}^3/\text{s}$, (Ref. 36), $k_{\text{rad}} = 3.0 \times 10^7\ \text{s}$ (Ref. 34), $k_{q,\text{He}} = 1.0 \times 10^{-12}\ \text{cm}^3/\text{s}$ (Ref. 28), and $k_{q,N_2} = 1.0 \times 10^{-10}\ \text{cm}^3/\text{s}$ (Ref. 28). Because $[N_2(C)] \ll [N_2(A)]$, the pseudo-steady-state approximation may be applied ($d[N_2(C)]/dt \approx 0$) and by solving for $[N_2(A)]$, one obtains:

$$[N_2(A)] \approx \sqrt{\frac{[N_2(C)](k_{\text{rad}} + k_{q,\text{He}}[\text{He}] + k_{q,N_2}[N_2])}{k_{\text{pool}}}} \qquad (2)$$

The largest value of the derivative in Eq. (1), $d[N_2(C)]/dt$, occurred immediately after turning off the rf power ($t = 0$ s). Including this derivative in the calculation resulted in a small change in the $N_2(A)$ concentration, ~0.01%. Thus, the pseudo-steady-state approximation was valid. The accuracy of the $N_2(A)$ concentrations obtained from the absorption measurements and from the $N_2(C)$ concentrations [i.e., Eq. (2)] was estimated to be within a factor of 2 of the real value.

2.5. N(^4S)

The $N_2(B)$ concentration in the late afterglow (where $[N_2(A)] \ll [N]$) depends on its rate of production by nitrogen atom recombination relative to its rate of consumption by collisional quenching (Table I).[37–39] Therefore, the nitrogen atom concentration was calculated from the $N_2(B)$ concentration as follows:

$$[N] \approx \sqrt{\frac{I_{N_2(B,v')} k_{\text{quench}}(v', \text{He})}{k_{\text{inst}} A(v', v'') k_{\text{recomb}}(v', \text{He})}}, \qquad (3)$$

Equation (3) was derived in a previous paper.[32] The intensity of the $N_2(B, 7)$ emission as a function of axial position in the late afterglow was monitored at 652 nm with the CCD as shown in Fig. 1a. The Einstein coefficient, $A(7, 4) = 9.61 \times 10^4\ \text{s}^{-1}$, the quenching rate constant, $k_{\text{quench}}(7, \text{He}) \approx k_{\text{quench}}(7, \text{Ar}) = 3.0 \times 10^{-13}\ \text{cm}^3/\text{s}$, and also the rate constant for N-atom recombination, $k_{\text{recomb}}(7, \text{He}) = 3.5 \times 10^{-35}\ \text{cm}^6/\text{s}$, were taken from literature.[28,32,34]

Table I. Reaction Mechanism for the Afterglow of the Nitrogen and Helium Atmospheric-Pressure Plasma

	Reaction	Rate constant (345 K)	(Ref.)
R_1	$N + N + He \rightarrow N_2(B) + He$	2.2×10^{-33} cm^6/s	32
R_2	$N + N + N_2 \rightarrow N_2(B) + N_2$	4.2×10^{-33} cm^6/s	19
R_3	$N_2(A) + N_2(A) \rightarrow N_2(B) + N_2$	1.1×10^{-9} cm^3/s	42
R_4	$N_2(A) + N_2(A) \rightarrow N_2(C) + N_2$	3.0×10^{-10} cm^3/s	36
R_5	$N_2(A) + N_2 \rightarrow N_2(X) + N_2$	4.0×10^{-17} cm^3/s	43
R_6	$N_2(A) + N \rightarrow N_2(X) + N$	9.6×10^{-11} cm^3/s	43
R_7	$N_2(B) \rightarrow N_2(A) + h\nu$	1.5×10^5 s	34
R_8	$N_2(B) + N_2 \rightarrow N_2(\neq B) + N_2$	3.0×10^{-11} cm^3/s	44
R_9	$N_2(B) + He \rightarrow N_2(\neq B) + He$	8.0×10^{-12} cm^3/s	45
R_{10}	$N_2(C) \rightarrow N_2(B) + h\nu$	3.0×10^7 s	34
R_{11}	$N_2(C) + N_2 \rightarrow N_2(\neq C) + N_2$	1.0×10^{-10} cm^3/s	33
R_{12}	$N_2(C) + He \rightarrow N_2(\neq C) + He$	1.0×10^{-12} cm^3/s	28

The $N_2(B)$ absolute emission technique is not valid in the early afterglow since the $N_2(B)$ can be produced by a variety of reactions (e.g., R_1, R_3, and R_4).[32] Therefore, a newly developed $N_2(B)$ temporal decay method was employed to extrapolate the N-atom concentration to the edge of the discharge. In this method, the nitrogen atom concentration was calculated from the following relationship[32]

$$[N(t)] = \frac{-d \ln I_{N_2(B,v')}(t)/dt}{4k_{recomb}(v', He)[He]}, \tag{4}$$

The emission intensity, $I_{N_2(B,7)}(t)$, was recorded at 652 nm with the PMT at times greater than 2 ms after extinguishing the discharge. To extrapolate to zero time, the following relationship was used,

$$\frac{1}{[d \ln I_{N_2(B,v')}(t)]/dt} = -\frac{1}{4k_{recomb}(v', He)[He][N(t_0)]} - \frac{t}{2} \tag{5}$$

A plot of $1/[d\ln(I_{N_2(B,v')}(t)]/dt)$ vs. t yielded a straight line with a slope of 0.5, and the initial concentration of nitrogen atoms, $[N(t_0)]$ can be extracted from the Y-intercept. The accuracy of these measurements was estimated to be $\pm 40\%$.

3. NUMERICAL MODEL

The afterglow chemistry and fluid mechanics encountered in the two-dimensional channel were modeled with FEMLAB, a partial differential equation solver utilizing the finite element method.[40] The inlet of the channel corresponded to the downstream edge of the rf powered electrode. The

model predictions were fitted to the experimental results by specifying the inlet conditions to the afterglow, including the gas velocity and the initial concentrations of He, N_2, $N(^4S)$, $N_2(A\,^3\Sigma_u)$, $N_2(B\,^3\Pi_g)$, and $N_2(C\,^3\Pi_u)$. Charged species were not included in the model, since their concentrations quickly drop from about 10^{11} cm^{-3} to $< 10^9$ cm^{-3} in a few microseconds.[17,32] Furthermore, we did not include vibrationally excited ground-state N_2, based upon the high pressure and low temperature of the discharge.[41]

No plug-flow assumptions were applied in the channel, so that the model included all mixing and viscous effects. It was assumed that the density and viscosity of the gas equaled that of pure helium, while diffusion coefficients were calculated for a helium and nitrogen mixture. The steady-state Navier-Stokes equation,

$$\rho(\nabla \cdot V)V = -\nabla p + \rho g + \mu(\nabla^2 u + \nabla^2 v), \tag{6}$$

and the species material balances,

$$V \cdot \nabla C_i = D(\nabla^2 C_i) + R_i \tag{7}$$

were solved simultaneously. The species material balances were not applied to He or N_2, because their concentrations were at least 100 times larger than the active species in the channel.

Presented in Table I is the reaction mechanism for the afterglow of the nitrogen and helium plasma. The generation and consumption terms, R_i, in Eq. (7) were compiled from the twelve reactions listed in this table.

4. RESULTS AND DISCUSSION

The optical emission spectra for the $\Delta v = 1$, 2, 3, and 4 transitions of $N_2(B)$ are shown in Fig. 2. These spectra were taken with the CCD collecting light from inside the plasma with a spectral resolution of 0.16 nm. In these figures, the intensity is corrected for the detector sensitivity as a function of wavelength. A weak helium atomic line can be seen at 706.5 nm. As can be seen, nitrogen atomic lines are not observed in these spectra. Even the atomic lines near 575.2 nm and the seven-line multiplet in the range of 818.5–824.2 nm, where the first positive emission is weak, cannot be detected.[46] For the vibrational sequence $\Delta v = 4$, the maximum intensity occurs at $v' = 7$. Although the Lewis–Rayleigh afterglow exhibits a maximum intensity at $v' = 11$, the presence of helium can shift this point to lower vibrational states.[47,48]

In Fig. 3, the species concentrations and the neutral temperature are plotted as functions of axial position and decay time in the afterglow. The open symbols correspond to measurements made along the length of the plasma during continuous operation, while the filled symbols represent

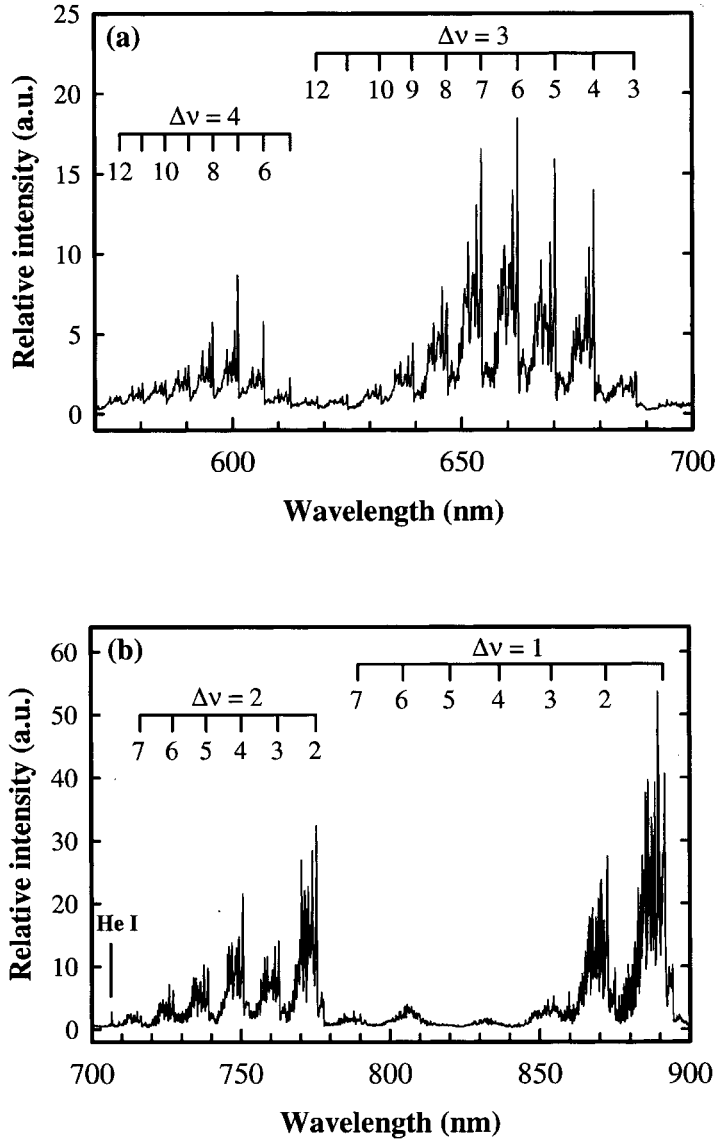

Fig. 2. Optical emission spectra of (a) the $\Delta v = 3$ and 4 transitions and (b) the $\Delta v = 1$ and 2 transitions for the first positive emission of nitrogen for operation with 10 Torr N_2, 750 Torr He and 15.5 W/cm^3 showing the absence of N atomic lines.

measurements obtained by pulsing the plasma. Axial positions below 0 cm are inside the discharge. In the afterglow, time has been mapped onto the position axis by multiplying the time elapsed after turning off the plasma by the linear velocity of the gas. The $N_2(B)$ species reaches its highest concentration, $1.2 \times 10^{12}\,cm^{-3}$, within 0.5 cm of entering the discharge. In the afterglow, the $N_2(B)$ concentration drops quickly within the first 2 ms and then falls more slowly with time. The $N_2(B)$ decay profile measured by pulsing the plasma agrees to within 8% of the spatial profile recorded during continuous operation (not shown).

The $N_2(C)$ species attains a maximum value of $3.2 \times 10^9\,cm^{-3}$ about 2 cm after entering the discharge. This trend is similar to that observed for the rotational temperature inside the plasma, which is about 375 K. Upon exiting the discharge, the $N_2(C)$ species decays extremely fast to $\sim 10^6\,cm^{-3}$ within only 2 ms. The $N_2(A)$ concentration has been measured for only a few positions near the exit of the atmospheric pressure discharge via ultraviolet absorption at 886 nm (□ symbols in Fig. 3). Here, the concentration equals $3.0 \times 10^{13}\,cm^{-3}$. Upon entering the afterglow, the density of $N_2(A)$ falls to $2 \times 10^{11}\,cm^{-3}$ in about 5 ms. Values obtained from Eq. (2) and the temporal

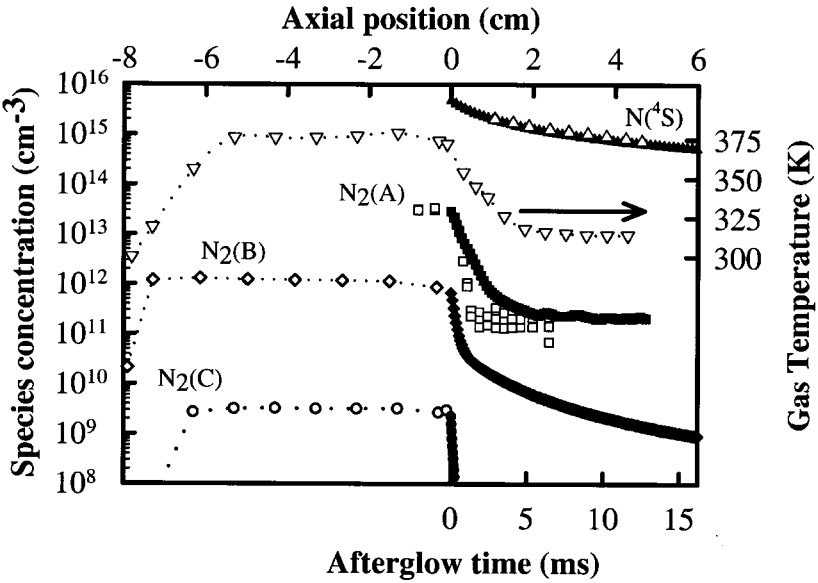

Fig. 3. The dependences of the $N(^4S)$, $N_2(A\,^3\Sigma_u)$, $N_2(B\,^3\Pi_g)$, and $N_2(C\,^3\Pi_u)$ concentrations and the neutral temperature on axial position in the plasma and afterglow decay time. See text for symbols.

decay of $N_2(C)$ (■ symbols in Fig. 3) are more accurate than those obtained from the absorption method. Nevertheless, the two techniques are in good agreement after ~4 ms.

The density of nitrogen atoms has been determined in the afterglow using Eqs. (3) and (4) (open and filled triangles, respectively). From 2 to 12 ms, these two methods provide the same results to within the experimental error of the measurement, < 10%. At the edge of the discharge, the N-atom concentration equals $4.8 \times 10^{15}\,cm^{-3}$, which is 100 times larger than the next most abundant species, $N_2(A)$. The nitrogen atoms decay more slowly than the other species, falling by only a factor of 5 in 5 ms, or 1.8 cm downstream. At this point, the density of the N atoms is approximately 10,000 times greater than that of the $N_2(A)$ molecules.

In Fig. 4, the results of the numerical simulations are compared to the experimental data collected by pulsing the plasma. The "best fit" is obtained by using the initial concentrations of $2.3 \times 10^{19}\,cm^{-3}$ He, $3.0 \times 10^{17}\,cm^{-3}$ N_2, $4.8 \times 10^{15}\,cm^{-3}$ of $N(^4S)$, $2.1 \times 10^{13}\,cm^{-3}$ $N_2(A\,^3\Sigma_u)$, $1.2 \times 10^{12}\,cm^{-3}$ $N_2(B\,^3\Pi_g)$, and $3.2 \times 10^{9}\,cm^{-3}$ $N_2(C\,^3\Pi_u)$. The decay profiles predicted by the model are in excellent agreement with the spectroscopic data. In the afterglow, nitrogen atoms are slowly consumed by the recombination reaction,

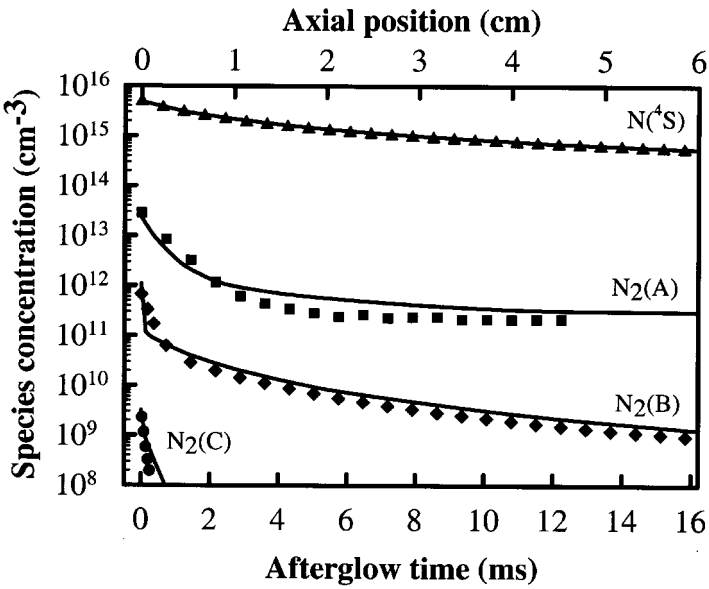

Fig. 4. Comparison of the concentration profiles of $N(^4S)$, $N_2(A\,^3\Sigma_u)$, $N_2(B\,^3\Pi_g)$, and $N_2(C\,^3\Pi_u)$ obtained from the experiments (symbols) and predicted by the numerical model (lines).

R_1 in Table I. The high concentration of nitrogen atoms causes a rapid decay of metastable nitrogen, $N_2(A)$, by R_6. Some $N_2(A)$ can be lost by the energy pooling reaction, R_4, but this is insignificant after about 5 ms in the afterglow. Note that the quenching of $N_2(A)$ by helium was not included in the model, since the rate constants could not be found, and this reaction is several orders of magnitude slower than R_6.[49,50]

The $N_2(B)$ and $N_2(C)$ species are mainly consumed by quenching with helium, R_9 and R_{12} in Table I, respectively. Quenching with nitrogen, R_8 and R_{11}, is not as important because the rate constants are an order of magnitude lower, and the concentration of helium is 75 times higher than that of nitrogen. Early in the afterglow, a small amount of $N_2(B)$ can be generated from the $N_2(A)$ pooling reaction, R_3. However, after 2 ms, the concentration of $N_2(B)$ is maintained by the recombination of nitrogen atoms. Based on the foregoing analysis, the mechanism may be simplified to five elementary reactions and still correctly predict the decay rates of the active species. These reactions are R_1, R_4, R_6, R_9, and R_{12}.

Shown in Fig. 5 are the dependences of the N and $N_2(A)$ concentrations at the plasma/afterglow boundary on the N_2 partial pressure. Both species densities increase gradually with the nitrogen pressure. The slopes of the trend lines from 0.7 to 12.0 Torr indicate that the nitrogen-atom concentration is proportional to $P_{N_2}^{0.71}$, while the $N_2(A)$ concentration is proportional to $P_{N_2}^{0.28}$. Above 12 Torr of N_2, the concentrations of both species decline. One possible explanation for this behavior can be obtained from Petov *et al.*,[24] who has modeled the effect of the nitrogen partial pressure on the electron density in helium and nitrogen atmospheric pressure plasmas. Their model indicates a maximum in the electron density near 0.1% nitrogen. Beyond this maximum, the concentration of the excited nitrogen species may decrease with the electron density. Instabilities in the plasma also could have caused the decrease in the $N_2(A)$ and N concentrations above 12 Torr. Increasing the nitrogen partial pressure above ~20 Torr in the present work, resulted in the appearance of obvious bright spots in the discharge region.

The effect of the rf power density on the N and $N_2(A)$ concentrations as well as the neutral temperature are shown in Fig. 6. The 15-degree rise in temperature does not appreciably effect the concentration of either species, since a separate experiment showed no change in concentration for either species upon changing the neutral temperature by 60 K with external cooling. From the slopes of the trend lines, the nitrogen atom density is proportional to $P_{rf}^{0.71}$, while the $N_2(A)$ density is proportional to $P_{rf}^{0.46}$. At the highest power density, 30.1 W/cm^3, the atmospheric pressure plasma generates 1.0×10^{16} cm^{-3} of N atoms. Beyond this power level, arcing occurs in the discharge region.

According to the literature, non-thermal nitrogen plasmas produce N-atom concentrations ranging from 10^{12} to $10^{16}\,cm^{-3}$.[15,16,19,27,29,38,51] These gas discharges are produced in microwave sources operating at 2.45 GHz in either pure nitrogen below 10 Torr, or in argon–nitrogen mixtures at atmospheric pressure. In the latter case, a surface wave discharge is produced by launching the wave electromagnetic field down a long glass tube 4 mm in diameter.[15,27,29] The different methods of ionizing the gases in these systems makes it difficult to compare their results to those presented herein. Nevertheless, it appears that the atmospheric pressure plasma examined in this study generates a relatively high concentration of nitrogen atoms, $\sim 10^{16}\,cm^{-3}$, at a low neutral gas temperature, 375 K.

Metastable-state molecular nitrogen is a relatively abundant species in nitrogen discharges. The concentration of $N_2(A)$ can range from 10^9 to $10^{14}\,cm^{-3}$.[16,35,36] At high pressures, this species is deactivated by collision with nitrogen atoms, R_6. With regard to $N_2(B)$ and $N_2(C)$, the concentrations of these species decrease with increasing pressure from 10 to 760 Torr.[19,38] This effect can be explained by the faster decay rates at high pressures due to collisional quenching with the background gas.

5. CONCLUSIONS

The concentration profiles of $N(^4S)$, $N_2(A\,^3\Sigma_u)$, $N_2(B\,^3\Pi_g)$, and $N_2(C\,^3\Pi_u)$ have been determined in the afterglow of a helium and nitrogen plasma operated at atmospheric pressure. Nitrogen atoms are the dominant species in the afterglow with a maximum concentration of $1.0 \times 10^{16}\,cm^{-3}$. After only 2 ms, the $N_2(A)$ concentration, the next most abundant species, is 1000 times smaller than that of the ground-state nitrogen atoms. The three-body recombination rate of N atoms is much slower than the collisional quenching rate of metastable N_2 molecules. These results can be applied to understanding the reaction pathways that occur in the atmosphere pressure PECVD of nitride materials.[52,53]

ACKNOWLEDGMENTS

This research was supported by grants from the UC SMART program, and the National Science Foundation, Division of Chemical and Thermal Systems.

REFERENCES

1. G. Lucovsky, H. Niimi, Y. Wu, C. R. Parker, and J. R. Hauser, *J. Vac. Sci. Technol.* A **16**, 1721 (1998).

2. C.-E. Morosanu, *Thin Solid Films* **65**, 171 (1980).
3. B. Monemar, *J. Mater. Sci: Mater. El.* **10**, 227 (1999).
4. A. Sherman, *Jpn. J. Appl. Phys.* **30**, 3553 (1991).
5. O. Ambacher, *J. Phys. D: Appl. Phys.* **31**, 2653 (1998).
6. J. W. Lee, K. D. MacKenzie, D. Johnson, J. N. Sasserath, S. J. Pearton, and F. Ren, *J. Electrochem. Soc.* **147**, 1481 (2000).
7. F. Delmotte, M. C. Hugon, and B. Agius, *J. Vac. Sci. Technol. B* **15**, 1919 (1997).
8. W. C. Hughes, W. H. Roland, Jr., M. A. L. Johnson, S. Fujita, J. W. Cook, Jr., J. F. Schetzina, J. Ren, and J. A. Edmond, *J. Vac. Sci. Technol. B* **13**, 1571 (1995).
9. M. A. Lieberman and A. J. Lichtenberg, *Principles of Plasma Discharges and Materials Processing*, John Wiley and Sons, Inc., New York, 1994.
10. S. E. Alexandrov, M. L. Hitchman, and S. H. Shamlian, *J. Mater. Chem.* **5**, 457 (1995).
11. B. F. Hanyaloglu and E. S. Aydil, *J. Vac. Sci. Technol. A* **16**, 2794 (1998).
12. D. C. Jordan, I. S. T. Tsong, D. J. Smith, B. J. Wilkens, and R. B. Doak, *Appl. Phys. Lett.* **77**, 3030 (2000).
13. Y. Manabe and T. Mitsuyu, *J. Appl. Phys.* **66**, 2475 (1989).
14. D. V. Tsu, G. N. Parsons, and G. Lucovsky, *J. Vac. Sci. Technol. A* **6**, 1849 (1988).
15. P. Merel, M. Tabbal, M. Chaker, M. Moisan, and A. Ricard, *Plasma Sources Sci. Technol.* **7**, 550 (1998).
16. C. Boisse-Laporte, C. Chave-Normand, and J. Marec, *Plasma Sources Sci. Technol.* **6**, 70 (1997).
17. V. Guerra and J. Loureiro, *Plasma Sources Sci. Technol.* **6**, 361 (1997).
18. P. A. Sa and J. Loureiro, *J. Phys. D: Appl. Phys.* **30**, 2320 (1997).
19. A. M. Diamy, L. Hochard, J. C. Legrand, and A. Ricard, *Plasma Chem. Plasma Process.* **18**, 447 (1998).
20. A. Schütze, J. Y. Jeong, S. E. Babayan, J. Park, G. S. Selwyn, and R. F. Hicks, *IEEE Trans. Plasma Sci.* **26**, 1685 (1998).
21. J. Y. Jeong, J. Park, I. Henins, S. E. Babayan, V. J. Tu, G. S. Selwyn, G. Ding, and R. F. Hicks, *J. Phys. Chem.* **104**, 8027 (2000).
22. J. Park, I. Henins, H. W. Herrmann, and G. S. Selwyn, *Phys. Plasmas* **7**, 3141 (2000).
23. S. E. Babayan, J. Y. Jeong, V. J. Tu, G. S. Selwyn, and R. F. Hicks, *Plasma Sources Sci. and Technol.* **7**, 286 (1998).
24. G. M. Petrov, J. P. Matte, I. Peres, J. Margot, T. Sadi, J. Hubert, K. C. Tran, L. L. Alves, J. Loureiro, C. M. Ferreira, V. Guerra, and G. Gousset, *Plasma Chem. Plasma Process.* **20**, 183 (2000).
25. G. Callede, J. Deschamps, and J. L. Godart, *Contrib. Plasma Phys.* **33**, 43 (1993).
26. V. Ya. Aleksandrov, D. V. Gurevich, I. V. Podmoshenskii, and S. F. Khlopina, *Sov. Phys. Tech. Phys.* **21**, 296 (1976).
27. A. Ricard, A. Besner, J. Hubert, and M. Moisan, *J. Phys. B: At. Mol. Opt. Phys.* **21**, L759 (1988).
28. E. Gat, N. Gherardi, S. Lemoing, F. Massines, and A. Ricard, *Chem. Phys. Lett.* **306**, 263 (1999).
29. G. Callede, J. Deschamps, J. L. Godart, and A. Ricard, *J. Phys. D: Appl. Phys.* **24**, 909 (1991).
30. J. Y. Jeong, S. E. Babayan, A. Schütze, V. J. Tu, J. Park, I. Henins, G. S. Selwyn, and R. F. Hicks, *J. Vac. Sci. Technol. A* **17**, 2581 (1999).
31. G. R. Rowlings, S. E. Babayan, V. Jankovic, and R. F. Hicks, *Plasma Sources Sci. Technol.*, scheduled for publication in February 2002.
32. S. E. Babayan, G. Ding, and R. F. Hicks, *Plasma Chem. Plasma Process.* **21**, 505 (2001).
33. M. Simek and S. De Benedictis, *Plasma Chem. Plasma Process.* **15**, 451 (1995).

34. F. R. Gilmore, R. R. Laher, and P. Espy, *J. Phys. Chem. Ref. Data* **21**, 1005 (1992).
35. G. Cernogora, L. Hochard, M. Touzeau, and C. Matos Ferreira, *J. Phys. B: At. Mol. Phys.* **14**, 2977 (1981).
36. L. G. Piper, *J. Chem. Phys.* **88**, 231 (1988).
37. A. Ricard, J. Tetreault, and J. Hubert, *J. Phys. B: At. Mol. Phys.* **24**, 1115 (1991).
38. J. F. Noxon, *J. Chem. Phys.* **36**, 926 (1962).
39. I. M. Campbell and B. A. Thrush, *Proc. Roy. Soc.* (*London*) **A296**, 201 (1967).
40. www.femlab.com
41. A. V. Pavlov and A. A. Namgaladze, *Geomagn. Aeron.* **28**, 607 (1988).
42. I. Nadler and S. Rosenwaks, *J. Chem. Phys.* **83**, 3932 (1985).
43. J. T. Herron, *J. Phys. Chem. Ref. Data* **28**, 1453 (1999).
44. L. G. Piper, *J. Chem. Phys.* **88**, 6911 (1988).
45. Y. Z. Ionikh and N. V. Chernysheva, *Opt. Spectrosc.* (*USSR*) **68**, 598 (1990).
46. J. Reader and C. H. Corliss, "Wavelengths and Transition Probabilities for Atoms and Atomic Ions." Washington, DC: U.S. Government Printing Office, 1980.
47. A. N. Wright and C. A. Winkler, "Active Nitrogen." New York: Academic Press, 1968.
48. M. Simek, G. Dilecce, and S. De Benedictis, *Plasma Chem. Plasma Process.* **15**, 427 (1995).
49. S. De Benedictis and G. Dilecce, *Plasma Sources Sci. Technol.* **4**, 212 (1995).
50. S. De Benedictis, G. Dilecce, and M. Simek, *Chem. Phys.* **178**, 547 (1993).
51. P. Supiot, O. Dessaux, and P. Goudmand, *J. Phys. D: Appl. Phys.* **28**, 1826 (1995).
52. O. Horie, P. Potzinger, and B. Reimann, *Chem. Phys. Lett.* **129**, 231 (1986).
53. L. G. Piper and G. E. Caledonia, *J. Phys. Chem.* **95**, 698 (1991).